THE JOURNAL OF BIOLOGICAL CHEMISTRY

Vol. 268, No. 7, Issue of March 5, pp. 4612–4621, 1993
Printed in U.S.A.

A Structural Difference between Filaments of Phosphorylated and Dephosphorylated *Acanthamoeba* Myosin II Revealed by Electric Birefringence*

(Received for publication, September 21, 1992)

Donald C. Rau‡§, Chhanda Ganguly¶, and Edward D. Korn¶

From the ‡Laboratory of Biochemistry and Metabolism, National Institute of Diabetes and Digestive and Kidney Diseases and the ¶Laboratory of Cell Biology, National Heart, Lung, and Blood Institute, National Institutes of Health, Bethesda, Maryland 20892

The actin-activated Mg^{2+}-ATPase activity of filamentous *Acanthamoeba* myosin II is regulated by the state of phosphorylation of three sites at the C terminus of each heavy chain. This phosphorylation at the tip of the tails of monomers in a bipolar filament abolishes the activity of sites some 90 nm distant in the globular heads. Previous studies with copolymeric filaments of phosphorylated and dephosphorylated monomers strongly indicated that the activity of each monomer in a filament is dependent on the level of phosphorylation of neighboring monomers in the filament. We report here electric birefringence measurements showing that, although the overall structures of phosphorylated and dephosphorylated filaments are very similar, large, Mg^{2+} concentration-dependent differences in internal motion and flexibility are observed. Filaments of dephosphorylated myosin II appear to be about 50-fold stiffer than filaments of phosphorylated myosin II at 4 mM Mg^{2+}. These results are consistent with a model in which the stiffness of the putative hinge region within the rod-like tail of each monomer is determined by the phosphorylation state of the C-terminal tails of overlapping, neighboring monomers. The flexibility of the filaments appears to be directly related to their actin-activated Mg^{2+}-ATPase activity.

Myosin II of *Acanthamoeba castellanii* is a conventional myosin with a pair of heavy chains of $M_r \sim 172{,}000$ and two pairs of light chains of $M_r \sim 17{,}500$ and $\sim 17{,}000$, respectively (1, 2). The ~90,000-Da N-terminal end of each heavy chain forms a globular head that contains the ATPase site and the ATP-sensitive, actin-binding site that regulates ATPase activity (3, 4). The remaining ~80,000 Da of each of the two heavy chains interact to form a coiled-coil, α-helical rod (2, 5) ending in a 29-residue, C-terminal non-helical tailpiece (5, 6). From the amino acid sequence (5), a bend (hinge) in the helical rod is predicted about 36 nm from the tip of the tail (or 40% of the distance from the end of the rod to the head/rod junction), and the bend has been observed in electron microscopic images of myosin II monomers (7).

The non-helical tailpiece of each heavy chain contains 3 serine residues at positions 1489, 1494, and 1499 from the N terminus (in reverse order, residues 11, 16, and 21 from the C terminus) that can be phosphorylated *in vivo* (8, 9) and by a specific myosin II heavy chain kinase (5, 6, 10, 11) *in vitro*. The actin-activated Mg^{2+}-ATPase activity that is maximally expressed by filamentous, dephosphorylated myosin II is almost totally inactivated by phosphorylation of these sites (10, 11), whereas Ca^{2+}-ATPase activity (10, 11) and the ability of the myosin to bind F-actin (12) are unaffected and minimally affected, respectively. Phosphorylation of Ser-1489 is sufficient to inactivate filamentous myosin II from which the 2 other phosphorylatable serine residues have been removed by limited proteolysis (13).

The actin-activated Mg^{2+}-ATPase activity of *Acanthamoeba* myosin II is maximally expressed in solutions containing 4–10 mM Mg^{2+}. Under these conditions, both active, dephosphorylated myosin II and inactive, phosphorylated myosin II are filamentous (7, 14), and only filamentous myosin II has been identified in the amoebae by immunoelectron microscopy (15). Thus, it is necessary to consider a mechanism by which phosphorylation of sites at the tip of the tails of monomers within a bipolar filament can regulate the actin-activated Mg^{2+}-ATPase activity at sites approximately 90 nm away in the globular heads without affecting the Ca^{2+}-ATPase activity and only minimally affecting the apparent affinity for F-actin at the same or neighboring sites.

A number of experimental results strongly suggest that the actin-activated Mg^{2+}-ATPase activity of each myosin II molecule in a filament is regulated by the level of phosphorylation of the filament as a whole rather than by its own phosphorylation state. For example, dephosphorylated myosin II is inhibited when copolymerized with phosphorylated myosin II (14) and phosphorylated myosin II is activated when copolymerized with *N*-ethylmaleimide-inactivated dephosphorylated myosin II (16). More specifically, dephosphorylated myosin II is inactivated when copolymerized with a phosphorylated ~28-kDa tail peptide derived from the C-terminal tail of myosin II by cleavage in the hinge region and phosphorylated myosin II is activated when copolymerized with the dephosphorylated tail peptide (17).

To approach the problem of myosin II filament structure, Wijmenga *et al.* (18) first studied the structure of monomers and parallel dimers by electric birefringence utilizing as a model system myosin II that been rendered incapable of forming filaments by chymotryptic removal of the C-terminal 66 amino acids (6, 7). They concluded that monomers in solution had on average an 110° bend at the hinge region, whereas at least one of the monomers in the dimer was straight while the other could be bent at an angle between 110° and 140°. From these data and from the stagger of the

* The costs of publication of this article were defrayed in part by the payment of page charges. This article must therefore be hereby marked "*advertisement*" in accordance with 18 U.S.C. Section 1734 solely to indicate this fact.

§ To whom correspondence should be addressed: Bldg. 10, Rm. 9B-07, National Institutes of Health, Bethesda, MD 20892. Tel.: 301-496-1241; Fax: 301-496-0839.

monomers in the parallel dimer (18) and the structure of bipolar filaments of myosin II deduced by Pollard (19) from electron microscopic images, Atkinson and Korn (20) proposed a filament model in which the hinge region of each monomer was adjacent to the phosphorylation sites of other monomers. As the non-helical tailpiece contains 5 arginine and 2 glutamic acid residues, the state of phosphorylation of the 3 serine residues would have a significant effect on the net charge at the C-terminal end of the rod. Thus, it was suggested (20) that changes in the average state of phosphorylation of the monomeric subunits could affect the conformation of the hinge region of other monomers in the filament and, as a consequence, possibly the way in which the globular heads at the N-terminal ends of the rods were presented to the actin filament, which might, in turn, regulate the actin-activated Mg^{2+}-ATPase activity.

We have now applied the electric birefringence technique to the study of filamentous *Acanthamoeba* myosin II. In addition to the overall rotation of filaments, internal motions within the filament are also observed. We find that dephosphorylated and phosphorylated myosin II are qualitatively similar structures but with an apparently large difference in internal flexibility in response to the electric field; filaments of dephosphorylated myosin seem to be about 50-fold more rigid under the experimental conditions. These results are consistent with a model in which the electric field perturbs a spring-like motion due to the flexing of the long HMM[1]-like arm at the hinge region, the flexibility of which is determined by the average state of phosphorylation of the overlapping C-terminal tails. The greater rigidity of filaments of dephosphorylated myosin II is, then, presumably directly related to their substantially higher actin-activated Mg^{2+}-ATPase activity.

MATERIALS AND METHODS

Myosin Preparations—Acanthamoeba myosin II was isolated (9) and dephosphorylated by potato acid phosphatase (8) as described. One portion of the dephosphorylated myosin II was phosphorylated with myosin II heavy chain kinase (10) using [γ-^{32}P]ATP. The dephosphorylated and phosphorylated myosins II were separated from acid phosphatase and heavy chain kinase, respectively, by gel filtration on Sepharose CL-4B equilibrated and eluted with 10 mM imidazole, pH 7.5, 0.6 M KCl, 1 mM EDTA, and 1 mM dithiothreitol (14). Fractions with Ca^{2+}-ATPase activity were pooled and dialyzed against 10 mM imidazole, 7.0, 0.1 M KCl, 10% sucrose, 1 mM dithiothreitol, concentrated against solid sucrose to a concentration of about 3 mg/ml, and stored on ice. The extent of heavy chain phosphorylation was quantified as described by Ganguly *et al.* (17). Routinely, the incorporation was 3–5 mol of phosphate/mol of myosin II. Chymotrypsin-treated myosin II was prepared as described by Côté *et al.* (6).

All myosin preparations were also characterized by their actin-activated Mg^{2+}-ATPase activity, which was determined as the difference in the rate of release of $^{32}P_i$ from [γ-^{32}P]ATP (21) when 80 nM myosin II filaments were incubated in the presence and absence of 15 μM rabbit skeletal muscle F-actin (22) at 30 °C in a buffer containing 10 mM imidazole, pH 7.0, 0.1 mM $CaCl_2$, 1 mM ATP, and either 4–5 mM $MgCl_2$ for dephosphorylated myosin II or 10 mM $MgCl_2$ for phosphorylated myosin II (12). Only samples of dephosphorylated myosin that were maximally active and phosphorylated myosin that were maximally inactive were used.

Myosin II samples for electric birefringence measurements were exhaustively dialyzed against 2.5 mM imidazole, pH 7.0, 5 mM KCl, 1 mM dithiothreitol, and 50% sucrose. Final protein concentrations were 1.4–1.5 mg/ml. After adjusting on ice to 1 mM imidazole, 1 mM KCl, 0.5 mM dithiothreitol, 5% sucrose, and between 30 and 140 μg/ml protein, $MgCl_2$ was added in aliquots (4–8, depending on the desired final Mg^{2+} concentration) with mixing. Especially at Mg^{2+} concentrations greater than 2 mM, direct addition of $MgCl_2$ in 1 aliquot occasionally resulted in slight visible turbidity that cleared only slowly and these samples often showed very slowly relaxing components in the birefringence experiments.

Electric Birefringence—The principles and practice of transient electric birefringence have been reviewed by Charney (23). The apparatus used in the experiments described here has been described elsewhere (18). Briefly, the optical train consists of a 10-milliwatt helium-neon laser (Uniphase), two high quality polarizers, and a $\lambda/4$ plate. The extinction coefficient of the system with crossed polarizers is routinely 1×10^{-6}. The light intensity detector is a high speed photodiode (EG&G HAD 1100A). The time constant of the photodiode and associated amplifiers is about 0.1 μs, determined from the birefringence signal from water. A Cober model 606 high voltage generator applies square wave electric field pulses to the sample. The optical signals are digitized and processed by a LeCroy transient recorder system controlled by an IBM PS/2 computer.

The major experimental difficulty encountered in the electric birefringence studies of *Acanthamoeba* myosin II filaments was that, at the comparatively high Mg^{2+} concentrations needed, the field strengths and pulse lengths necessary for significant orientation resulted in field-induced changes in the signal that accumulated with increasing signal averages. With extended pulsing or very high field strengths (>5 kV/cm), the solutions became visibly turbid and signal amplitudes varied greatly with very slow and irreproducible kinetics. This limited the field strengths and pulse lengths that could be applied, the number of pulses that could be averaged, and, therefore, the quality (signal to noise ratio) of the data. Applied pulse lengths of 120–150 μs were our compromise between amplitude and signal/noise ratio. As will be presented later, signal amplitudes showed low field, Kerr law behavior (linearly proportional to E^2, where E is the applied field strength) and scaled linearly with myosin concentration. Within the constraints on field strength and pulse length imposed by the system, myosin II filaments were well behaved, with no evidence for field induced irreversible changes in structure during an experiment.

Data Analysis and Calculations—Data manipulation and analysis were done using SigmaPlot 5.0 (Jandel Scientific Corp.) and MathCad 3.1 (Mathsoft Inc.). Decay rates were also analyzed using the Fortran program Contin (24, 25). This software determines the best fitting spectrum of exponential relaxation times by an inverse LaPlace transform of the data. The slow relaxation rates were determined directly from data spanning the time range 150 μs to 2.5 ms after the end of the pulse. For the same sample, exponential fits, semilog plot slopes, and Contin all gave the same relaxation time to within 10%. Extracted slow component relaxation times were the same for baseline values directly calculated from the data and for baseline values determined by fitting exponential decays. Fast relaxation rates were estimated either by subtracting the slow component and integrating the area under the resulting normalized decay curve or by a two-peak-constrained Contin analysis. The methods agreed to within about 25% for the average fast component relaxation time.

Rotational friction coefficients were calculated as described by Garcia de la Torre and Bloomfield (26). Octameric myosin II filaments were constructed by tight packing of the monomer bead model described in Wijmenga *et al.* (18). The relative angular orientation of the globular heads and the bend angle of the HMM-like regions with respect to the long filament axis were varied. The Fortran program uses a Gauss-Siedel iterative procedure for calculating frictional coefficients from self-consistent hydrodynamic interactions between beads.

RESULTS

Comparison of the Electric Birefringence Signals from Monomeric and Filamentous Myosin II—Birefringence signals observed for *Acanthamoeba* myosin II minifilaments are so fundamentally different from the myosin monomer and parallel dimer signals reported by us previously (18) that a comparison is necessarily instructive. Fig. 1 shows a typical electric birefringence signal from monomeric myosin II (chymotrypsin-treated to prevent filament formation at low salt concentrations) at a concentration of 35 μg/ml in 1 mM KCl, 1 mM imidazole, pH 7.0, 0.5 mM dithiothreitol, and 5% sucrose. Since the coiled-coil α-helices of the rod-like tails are expected to dominate the optical signal, the positive sign of the birefringence indicates that monomers are orienting with their long axes parallel to the applied field.

[1] The abbreviations used are: HMM, heavy meromyosin; LMM, light meromyosin.

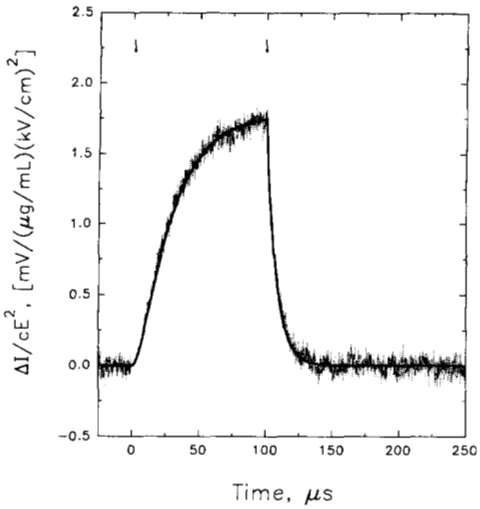

FIG. 1. **The electric birefringence signal of monomeric *Acanthamoeba* myosin II.** Chymotrypsin-treated myosin at 35 μg/ml in 1 mM KCl, 1 mM imidazole, pH 7.0, 0.5 mM dithiothreitol, and 5% sucrose was oriented in a 1 kV/cm field at 20 °C. The signal shown is the average of 32 pulses. The start of the square wave pulse is at 0 μs and the end at about 100 μs (indicated by the *arrows*). Signal amplitudes are normalized for protein concentration and field strength. The *solid line* is the best fit to the data assuming only a permanent dipole and a rotational relaxation time of 8.9 μs in 5% sucrose. Similar data have been published previously (18).

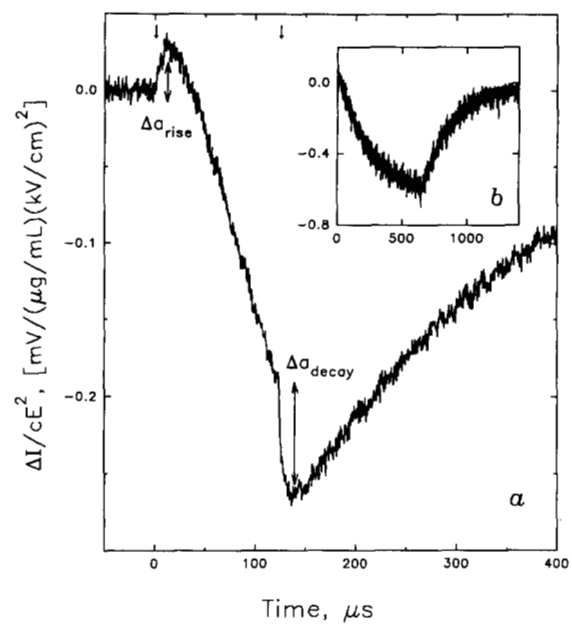

FIG. 2. **The electric birefringence signal of filamentous *Acanthamoeba* myosin II.** Phosphorylated myosin at 75 μg/ml in 1 mM KCl, 1 mM imidazole, pH 7.0, 0.5 mM dithiothreitol, 2 mM $MgCl_2$, and 5% sucrose was oriented in a 2 kV/cm field at 20 °C. The signal shown in *a* is the average of 16 pulses. The start of the pulse is at 0 μs and the end at about 120 μs (indicated by the *arrows*). Signal amplitudes are normalized for protein concentration and field strength. The sum of the fast, positive and slow, negative birefringence components gives the maximum observed in the rise with amplitude $\Delta\sigma_{rise}$ and the minimum seen in the decay with amplitude $\Delta\sigma_{decay}$. The *inset* (*b*) shows the birefringence signal normalized for protein concentration and field strength with a single 650-μs pulse at 2 kV/cm.

The decay of the signal can be well described by a single exponential with a time constant of 7.8 μs (corrected to water viscosity), in good agreement with the value of 8 μs reported by us previously (18). This relaxation time corresponds to rotational diffusion of monomers about their long axes. The rate of signal rise with applied field is much slower than the decay rate after the field is removed. This is indicative of a permanent dipole mechanism of orientation. The *solid line* in Fig. 1 shows the best fit of the data to a classical permanent dipole mechanism (27) with no contribution from an induced dipole moment.

The distribution of charged amino acids in the sequence reported by Hammer *et al.* (5) for *Acanthamoeba* myosin II predicts a substantial permanent dipole over the N-terminal 1250 amino acids of the molecule (the globular heads and the N-terminal 50 nm of the rod-like tails). Since the dipole magnitude cannot be separated from the intrinsic optical factor of the myosin rods at these field strengths, however, we cannot quantitatively compare the permanent dipole underlying the orientation in the birefringence experiment with the expected dipole from the amino acid sequence.

Fig. 2 shows typical birefringence signals at 20 °C for filamentous phosphorylated myosin II at 75 μg/ml, in 1 mM imidazole, pH 7.0, 1 mM KCl, 0.5 mM dithiothreitol, 5% sucrose, and 2 mM $MgCl_2$. As discussed under "Materials and Methods," pulse lengths long enough for the filaments to reach a steady state orientation also cause significant signal degradation after only a few pulses. The 120-μs pulse length data averaged over 16 pulses shown in Fig. 2*a* is our compromise between signal amplitude and signal/noise ratio. A signal from a single 650-μs pulse is shown in Fig. 2*b*.

At least two components can be observed in the filament signal. The dominating component at long times shows negative birefringence. At very early times, however, a positive birefringence component with much smaller amplitude is observed in both the rise and the decay.

An important difference between the filament and monomer signals is that the signs of the major components are opposite. This change in sign of the birefringence indicates that the long axis of the filament orients perpendicularly to the applied field. Furthermore, the rise rate of this slow component is not significantly slower than the decay rate (see Fig. 2*b*), *i.e.* there is no large fixed permanent dipole that orients filaments. The permanent dipole contributions from the subunits will exactly cancel for centrosymmetric, bipolar structures.

Analysis of Filament Relaxation Times—Semilog plots of the decay of the slow, major component of the electric birefringence signal for three concentrations of myosin II filaments are shown in Fig. 3. The relaxation of the negative birefringence signal is well described by a single exponential with a decay time, τ_{slow}, of 215 ± 20 μs (corrected to water viscosity). Analysis of the data by Contin (24, 25) shows a narrow distribution of relaxation times centered about 220 μs. The slow component relaxation times are not dependent on the applied field strength (up to about 4 kV/cm) or pulse length from 2 to 650 μs. There is no apparent dependence of the relaxation time on myosin concentration between 40 and 140 μg/ml. As we shall discuss below, the observed relaxation time is consistent with rotational diffusion coefficients calculated for the minifilament structures determined by electron microscopy.

In addition to the major, slow component, a positive birefringence component of smaller amplitude and much faster kinetics is apparent in the filament signal. This signal arises either from internal filament motions or from the fast rotation of myosin species other than filaments, *e.g.* unpolymerized monomers or partially assembled filaments. The decay kinetics of the fast, positive birefringence component are more difficult to extract, requiring either subtracting the slow com-

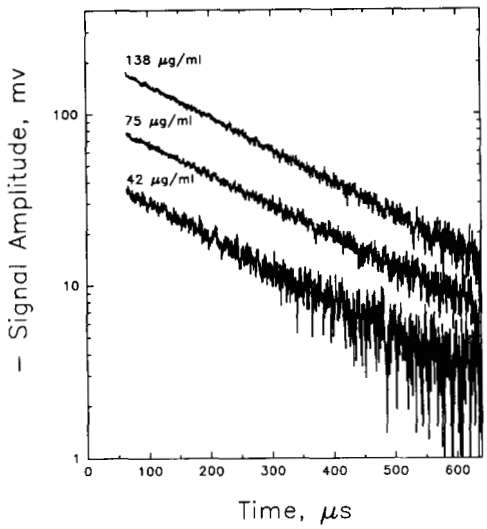

FIG. 3. **The slow component relaxation of filamentous phosphorylated myosin II is single exponential with a decay time independent of protein concentration.** Semilog plots of signal amplitude *versus* time for the birefringence decay of three concentrations of myosin (indicated in the figure) at 20 °C and in 1 mM KCl, 1 mM imidazole, pH 7.0, 0.5 mM dithiothreitol, 2 mM $MgCl_2$, and 5% sucrose are shown. The applied field for all three was 2 kV/cm. Relaxation times are proportional to the inverse of the slopes. In 5% sucrose, the observed τ_{slow} = 245 ± 25 μs or 215 μs corrected to water viscosity at 20 °C.

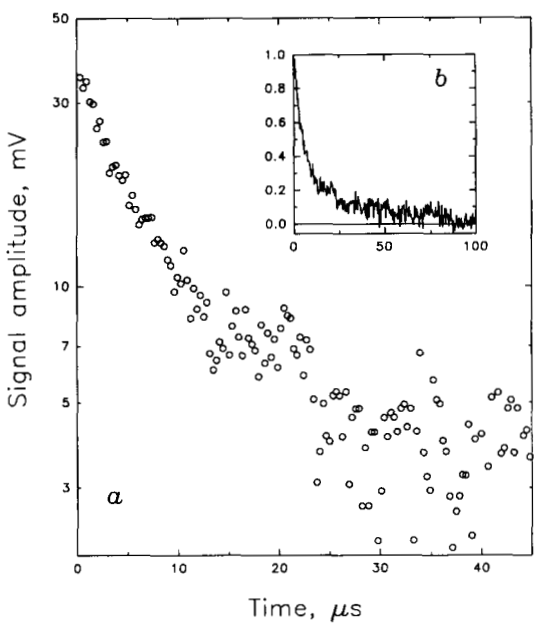

FIG. 4. **The fast component relaxation is not well defined.** A semilog plot of signal amplitude of the fast component decay *versus* time is shown in *a* for filamentous phosphorylated myosin II at 20 °C and 100 μg of protein/ml, in 1 mM KCl, 1 mM imidazole, pH 7.0, 0.5 mM dithiothreitol, 2 mM $MgCl_2$, and 5% sucrose. The best fitting exponential decay for the slow component at long times (Fig. 3) is subtracted from the early time data. Signal amplitude, normalized by the amplitude at $t = 0$, *versus* time is shown in *b*. The area under this curve defines the average, fast component relaxation time, $\langle\tau_{fast}\rangle$, and is 13.5 μs for the data shown.

ponent kinetics from the total curve, using double exponential fits, or applying peak-constrained Contin analyses. Fig. 4*a* shows a semilog plot of the fast component kinetics after subtracting the slow component decay. The substantial curvature observed indicates that the fast component does not have a well defined relaxation time. The average fast component relaxation time, $\langle\tau_{fast}\rangle$, from integrating the area under a normalized stripped decay curve (Fig. 4*b*) is 13 ± 2 μs. A two-peak-constrained Contin analysis without subtracting the slow component decay also shows a spectrum of decay rates ranging from about 5 to 50 μs, with an amplitude weight average relaxation time of 15 ± 5 μs. A broad distribution of relaxation rates such as this means either several different filament internal motions are perturbed by the electric field or several distinct myosin species, with different rotational diffusion coefficients, are present, or both.

Separate amplitudes for the fast and slow components can be extracted by fitting the slow decay kinetics to a single exponential. Fig. 5 (*a* and *b*) shows the field strength and myosin concentration dependence values of the fast and slow component amplitudes, respectively. Up to field strengths (E) of about 3–4 kV/cm, the amplitudes of both vary as E^2, consistent with low field, Kerr law behavior (the orientation energy is small compared with thermal energy). In the range 40–140 μg of protein/ml, the amplitudes of the two components are directly proportional to concentration. The ratio of fast to slow component amplitudes ($\Delta a_{fast}/\Delta a_{slow}$) is constant

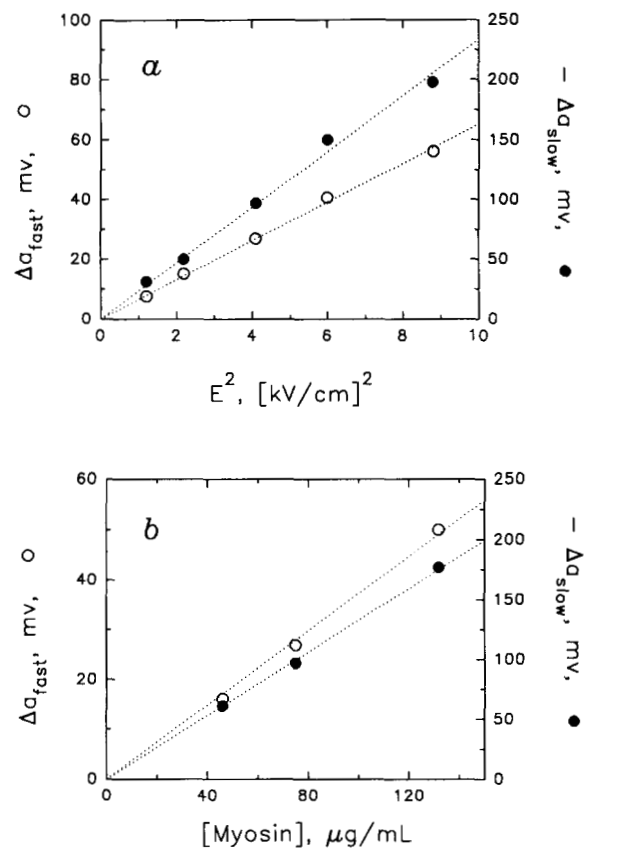

FIG. 5. **The dependence of signal amplitude for separated fast and slow components on field strength, E, and myosin II concentration.** The birefringence of filamentous phosphorylated myosin II was measured at 20 °C in 1 mM KCl, 1 mM imidazole, pH 7.0, 0.5 mM dithiothreitol, 2 mM $MgCl_2$, and 5% sucrose with a 120-μs pulse length. Total signal amplitudes were separated into fast and slow component contributions by fitting the slow component to a single exponential decay. In *a*, signal amplitudes for 75 μg/ml of myosin are shown as a function of E^2, illustrating limiting Kerr law behavior. In *b*, signal amplitudes at 2 kV/cm are seen to be linearly dependent on myosin concentration. In both panels, *open circles* (○) refer to the fast component and *closed circles* (●) to the slow. The error in determining separated amplitudes is about 10%, estimated from three separate experiments. The *dotted lines* are the best fitting straight lines that extrapolate to amplitude = 0 at E = 0 or at [myosin] = 0.

and equal to about 0.28 ± 0.02, independent of field strength and myosin concentration.

Differences between the rise and decay kinetics give information about the origin of the dipole moment. For low field strengths (Kerr region), molecules with purely classical induced dipoles show symmetric rise and decay kinetics. At the other extreme, molecules with only a fixed permanent dipole show a lag in the rise kinetics that correlates with the rotational kinetics of the molecule. The rise kinetics of the slow filament component alone can be extracted by varying the orienting pulse length and determining the amplitude of the slow component by fitting the decay to a single exponential. Fig. 6 shows the extracted rise kinetics for the slow and fast components determined by this method. A distinct lag of about 10 μs is observed in the rise of the slow component. The time constant of the lag correlates with the average rise time of the fast component. A much longer lag time of about 80 μs would be expected for a molecule with a fixed permanent dipole and 240-μs rotational relaxation time. The most straightforward interpretation of this lag and its correlation with the fast component kinetics is that the orientation of the slow component is caused by a dipole induced by the fast motions. Szabo *et al.* (28) have derived equations for rotational orientation coupled with "slow" (not instantaneous) induced dipole kinetics. The *solid line* in Fig. 6 shows the best fit to the slow component data, with solution viscosity-corrected relaxation times of τ_{dipole} = 15 μs (the fitted parameter) and τ_{slow} = 220 μs (taken from experiment). The close correspondence of τ_{dipole} with the average fast component kinetics ($\langle\tau_{fast}\rangle$ ~ 13 μs) leads to the conclusion that the fast and slow components are coupled. Thus, it appears that at least some part of the observed fast kinetics is due to internal motions

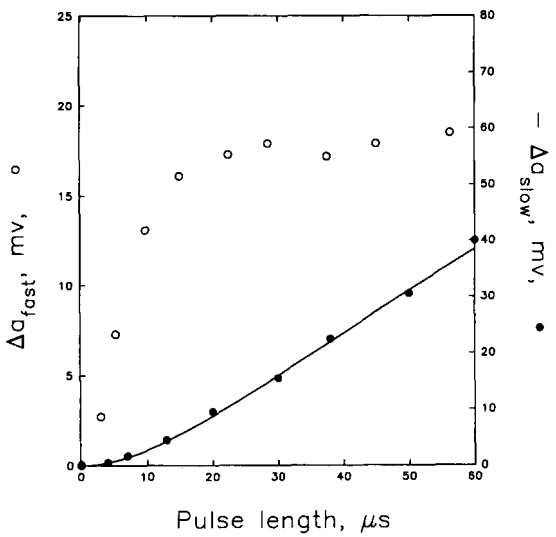

FIG. 6. **The birefringence rise kinetics of separated fast and slow components.** Signal amplitudes of separated fast (○) and slow (●) components are shown as a function of orienting pulse length. Filamentous phosphorylated myosin II at 75 μg/ml and 20 °C was oriented with a 2 kV/cm field pulse in 1 mM KCl, 1 mM imidazole, pH 7.0, 0.5 mM dithiothreitol, 2 mM $MgCl_2$, and 5% sucrose. Signal amplitudes are extracted by fitting the slow component starting at 75 μs after the end of the pulse to a single exponential decay. Since many more pulses can be signal-averaged at these pulse lengths (the 12-μs pulse data points, for example, are from the average of 128 pulses), the error in signal amplitude is about 0.5 mV independent of absolute amplitude. The *solid line* shows the best fit to the slow component data of the equations given by Szabo *et al.* (28) for a slow induced dipole coupled to the rotation of a rod-like molecule. The parameters (for 5% sucrose viscosity) used are τ_{rot} = 250 μs and τ_{dipole} = 17 μs.

within the filament (and not to other species) that result in a net dipole for filament orientation. In spite of this lag in the slow component rise, however, the amplitude difference between the start of the pulse and the maximum amplitude in the rise (Δa_{rise} in Fig. 2*a*) is small compared with the amplitude difference between the end of the pulse and the decay minimum (Δa_{decay}). The ratio, $\Delta a_{rise}/\Delta a_{decay}$, is only about 0.18 ± 0.02. If only the slow component is affected by this coupling of kinetics, this ratio would be greater than 1.0. That it is much less means the fast kinetics are also convoluted with the slow.

Comparison of Filaments of Phosphorylated and Dephosphorylated Myosin II—With the foregoing analysis of the general features of the electric birefringence of filaments, we can now systematically evaluate the effects of myosin phosphorylation. Fig. 7 compares signals from dephosphorylated myosin II filaments with the curve given in the previous section for phosphorylated myosin at 2 mM $MgCl_2$ (with 1 mM KCl, 1 mM imidazole, pH 7.0, 0.5 mM dithiothreitol, and 5% sucrose). Aside from the marked difference in amplitudes (about a factor of 4–5), the two signals are qualitatively very similar. Like phosphorylated filaments, the amplitudes of the fast and slow components for dephosphorylated myosin filaments also are linearly proportional to myosin concentration and show a limiting Kerr region E^2 field strength dependence (data not shown). Over the number of pulses averaged and field strengths applied, there was no indication of signal degradation. In spite of the large change in amplitude, the ratio of fast and slow component amplitudes ($\Delta a_{fast}/\Delta a_{slow}$) for dephosphorylated myosin filaments (0.32 ± 0.06) is only slighter larger than for phosphorylated filaments (0.28 ± 0.02).

Semilog plots of the the slow component decays from phosphorylated and dephosphorylated myosin filaments in 2 mM Mg^{2+} are shown in Fig. 8*a*. Both can be well described by single exponential relaxations with very similar relaxation times, τ_{slow} = 230 μs for filaments of dephosphorylated myosin and 215 μs for phosphorylated myosin (both corrected to water viscosity). Although the difference is within experimen-

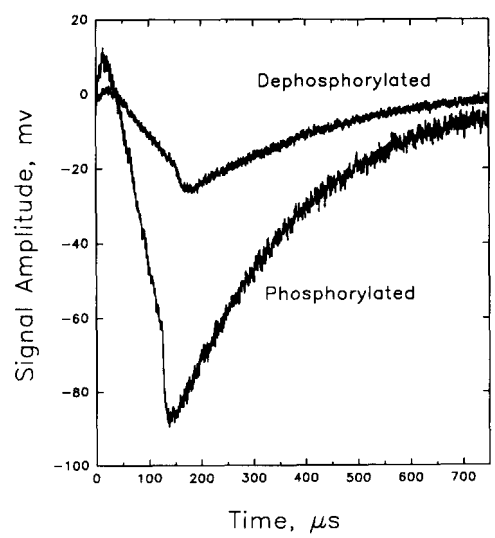

FIG. 7. **A comparison of birefringence signals of phosphorylated and dephosphorylated myosin II filaments.** Signal amplitudes *versus* time are shown for a field strength of 2 kV/cm, at 20 °C, in 1 mM KCl, 1 mM imidazole, pH 7.0, 0.5 mM dithiothreitol, 2 mM $MgCl_2$, and 5% sucrose. For both, the myosin concentration is 75 μg/ml. The start of the square wave field pulse is at time = 0. The pulse length is 120 μs for the phosphorylated myosin data (16 pulse average) and 150 μs for the dephosphorylated myosin data (32 pulse average).

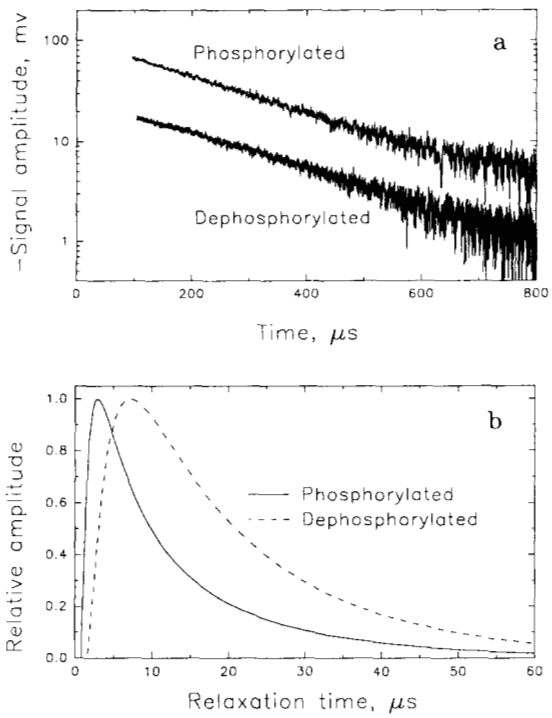

FIG. 8. **A comparison of the slow and fast component relaxation rates for phosphorylated and dephosphorylated myosin II filaments.** *a*, semilog plots of signal amplitude *versus* time are shown for the slow component decay data of Fig. 7. Both can be well described by a single exponential decay with relaxation times in 5% sucrose of 245 and 265 μs for phosphorylated and dephosphorylated myosin filaments, respectively. *b*, the spectrum of relaxation times characterizing the fast component was extracted from the decay data shown in Fig. 7 by a two-peak-constrained Contin analysis. No subtraction of the slow component decay is involved. The relative amplitude or probability of observing a particular relaxation time (normalized such that the peak is 1.0) is shown as a function of relaxation time. The average fast component relaxation times calculated from the peak-constrained Contin spectrum and from the area under the normalized fast component decay with the slow component decay subtracted are 15 and 13 μs for phosphorylated myosin II filaments and 35 and 28 μs for dephosphorylated filaments.

tal error (about 10%), it was reproducible. Given the sensitivity of rotational diffusion coefficients to long axis dimensions, this small difference would reflect only very small differences in structure. Thus, the basic structure of filaments is insensitive to myosin phosphorylation.

Although we cannot determine the kinetics of the fast component with as much accuracy as for the slow component, there are significant qualitative changes in the spectrum of fast relaxation times between phosphorylated and dephosphorylated myosin filaments. Fig. 8*b* shows a comparison of relaxation time spectra derived from two-peak-constrained Contin analyses of the data obtained at 2 mM Mg^{2+}. Both phosphorylated and dephosphorylated filaments show a relatively broad spectrum of relaxation times. There is, however, a significant shift in the distribution. The average decay rate for dephosphorylated myosin filaments is significantly longer than for phosphorylated filaments. The average fast component relaxation time, $\langle \tau_{fast} \rangle$, is 28 ± 8 μs for dephosphorylated myosin filaments, compared with 13 ± 2 μs for phosphorylated filaments. This difference can be directly observed in the birefringence curves. The position of the minimum in the decay is determined both by the relative amplitudes and by the relative relaxation times of the two components. For dephosphorylated myosin, this minimum occurs at about 25 ± 6 μs after the end of the pulse compared to about 12 ± 2 μs for phosphorylated filaments. Since the ratios of fast to slow amplitudes and the slow relaxation times are nearly the same for the two filaments, this difference in position of the minimum in the decay can only be due to a difference in fast component kinetics. There is also observed a change in the ratio of the amplitude at the rise maximum to the decay minimum amplitude, $\Delta a_{rise}/\Delta a_{decay}$. In contrast to the observed ratio of 0.18 ± 0.02 for phosphorylated myosin, a value of 0.4 ± 0.1 is seen for dephosphorylated filaments.

Fig. 9 shows the amplitudes of the slow components for phosphorylated and dephosphorylated myosin filaments as dependent on Mg^{2+} concentration. At 1 mM Mg^{2+}, there is only about a 25% difference in slow component amplitude for the two filaments. By 4 mM, however, there is about a 50-fold difference in amplitude. This change in relative amplitude is predominately due to a dramatic decrease in dephosphorylated filament amplitude. There is a relatively small, 25% increase in the slow component amplitude for phosphorylated myosin between 1 and 4 mM Mg^{2+}. Changes in the fast component amplitude are well correlated with the slow component. The ratio $\Delta a_{fast}/\Delta a_{slow}$ is fairly constant, 0.30 ± 0.05, independent of Mg^{2+} and overall signal amplitude for both phosphorylated and dephosphorylated filaments.

The relaxation time of the slow component is essentially constant for phosphorylated filaments between 1 and 4 mM Mg^{2+}, ranging from 210 μs at 1 mM to about 220 μs at 4 mM (with about 10% experimental error). Significant changes (>~30%) in fast component kinetics are not observed (data not shown).

At 1 mM Mg^{2+}, the slow relaxation time for dephosphorylated filaments is 215 μs. The average fast component relaxation time, $\langle \tau_{fast} \rangle$, is about 18 ± 5 μs. The ratio of rise maximum amplitude to decay minimum, $\Delta a_{rise}/\Delta a_{decay}$, is 0.25 ± 0.03. Both these latter two parameters are significantly smaller at

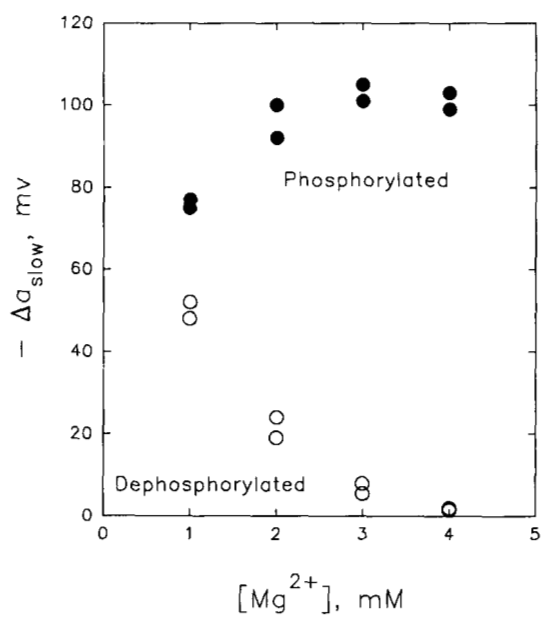

FIG. 9. **A comparison of the dependence of slow component amplitudes on Mg^{2+} concentration for phosphorylated and dephosphorylated myosin II filaments.** Slow component amplitudes extracted from fitting long time decays to single exponentials *versus* Mg^{2+} concentration are shown for a 2 kV/cm field strength and 120-μs pulse length at 20 °C and 75 μg protein/ml. In addition to Mg^{2+}, the buffer also contained 1 mM KCl, 1 mM imidazole, pH 7.0, 0.5 mM dithiothreitol, and 5% sucrose. The *open circles* (○) indicate phosphorylated myosin and *closed circles* (●) dephosphorylated. Each *point* is the average of 2 experiments on a single myosin preparation.

1 mM Mg^{2+} than at 2 mM Mg^{2+}, and more like those found for phosphorylated filaments. At 3 mM Mg^{2+}, the kinetic parameters for filamentous, dephosphorylated myosin are little different from 2 mM, with $\tau_{slow} = 230 \pm 30$ μs, $\langle\tau_{fast}\rangle = 31 \pm 10$ μs, and $\Delta a_{rise}/\Delta a_{decay} = 0.43 \pm 0.15$. Since the signal amplitudes were so small, we cannot determine with accuracy either the slow relaxation component or the fast kinetics of dephosphorylated myosin filaments at 4 mM Mg^{2+}. The observed slow relaxation at this concentration, however, is consistent with an approximate 200–250-μs decay time.

Copolymeric Filaments—The actin-activated Mg^{2+}-ATPase activity of mixed copolymers of phosphorylated and dephosphorylated myosin shows a distinctive nonlinear dependence on the fraction of phosphorylated myosin (14). The electric birefringence of copolymeric filaments shows a similar behavior. Fig. 10 shows the slow component amplitude at 3 mM Mg^{2+} as a function of the fraction of phosphorylated myosin. Fast component amplitudes are well correlated with these slow relaxation amplitudes, with $\Delta a_{fast}/\Delta a_{slow} = 0.30 \pm 0.04$ for all data shown in Fig. 10. Slow component amplitudes of copolymers are not a simple linear function of the fraction of phosphorylated myosin. At any given fraction of phosphorylated myosin, the slow component amplitude is greater than expected for a simple linear average. The *solid line* shows that a simple quadratic dependence of amplitude on the fraction of dephosphorylated monomer, however, can adequately describe the curve.

Fig. 11*a* shows that the slow component relaxation time is, within experimental error, constant, independent of the fraction of phosphorylated myosin. Thus, there is no apparent

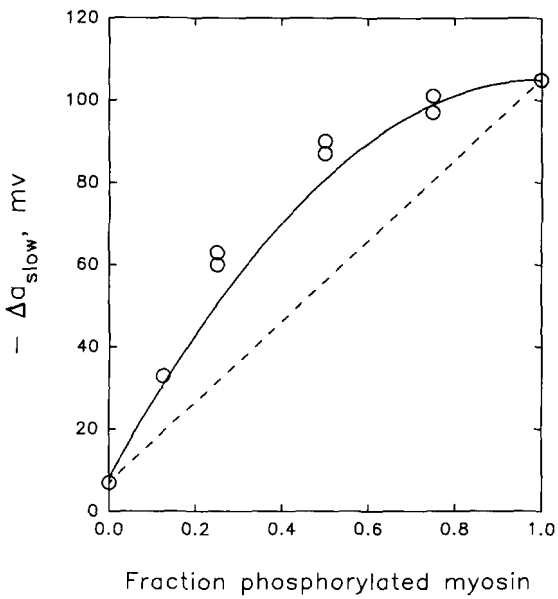

FIG. 10. **The dependence of the slow component amplitude of copolymeric filaments on the fraction of phosphorylated myosin II.** Copolymeric filaments are made by mixing phosphorylated and dephosphorylated myosin in 5 mM KCl, 2.5 mM imidazole, pH 7.0, 1 mM dithiothreitol, and 50% sucrose, then diluting to 1 mM KCl, 1 mM imidazole, 0.5 mM dithiothreitol, 3 mM $MgCl_2$, and 5% sucrose with a final myosin concentration of 75 μg/ml. The field strength was 2 kV/cm with a 120-μs pulse. Slow component amplitudes were extracted by fitting decays to single exponentials. Each *point* is the average of two experiments on a single set of myosin preparations. The *two endpoints* are the average of five experiments. The *dashed line* is the expected result for a linear dependence between Δa_{slow} and fraction of phosphorylated myosin, whereas the *solid line* is the expected curve for the next higher order dependence, a quadratic function, *i.e.* $\Delta a_{slow,copoly} = 8(f_{dephos})^2 \pm 105(1 - (f_{dephos})^2)$, where f_{dephos} is the fraction of dephosphorylated myosin.

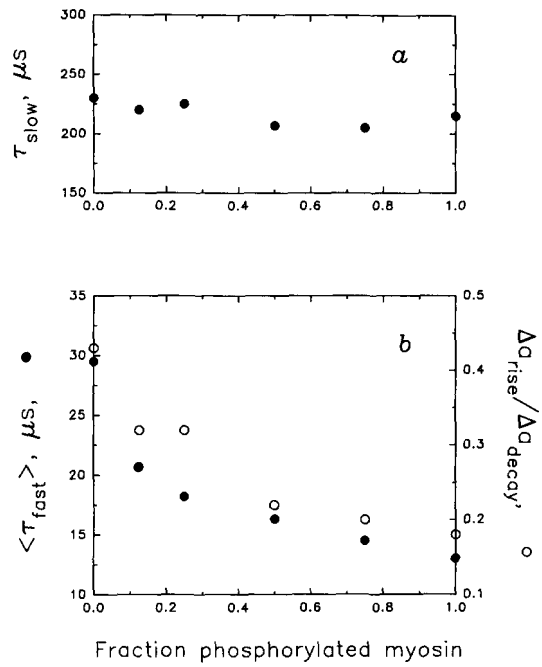

FIG. 11. **The dependence of relaxation rate parameters of copolymeric filaments on the fraction of phosphorylated myosin II.** Experimental conditions are the same as in Fig. 10. The variation of the slow component relaxation time, extracted from single exponential fits to the decay, on the fraction of phosphorylated myosin is shown in *a*. The error is about 10%. In *b*, the dependence of the average fast component relaxation time, *closed circles* (●), and the ratio of the rise maximum to decay minimum, $\Delta a_{rise}/\Delta a_{decay}$, *open circles* (○), on fraction of phosphorylated myosin is shown. The average fast component relaxation time, $\langle\tau_{fast}\rangle$, was determined from area under the normalized decay curve after subtracting the slow component exponential decay. The estimated error is about 25%. The $\Delta a_{rise}/\Delta a_{decay}$ was determined directly from the birefringence curves and has an error of about 10%.

difference in overall structure as seen by the rotational diffusion coefficient. Fig. 11*b* shows the average fast component relaxation time, $\langle\tau_{fast}\rangle$, and the ratio of the rise maximum amplitude to decay minimum, $\Delta a_{rise}/\Delta a_{decay}$, as functions of the fraction of phosphorylated myosin. Both these parameters show a significant dependence on the fraction of phosphorylated monomer. As with signal amplitudes, this dependence is clearly nonlinear and is dominated by the fraction of phosphorylated monomer.

DISCUSSION

The assembly of *Acanthamoeba* myosin II monomers into filamentous structures is sensitive to the concentrations of KCl, pH, Mg^{2+}, and sucrose. In general, filament formation is favored by low ionic strengths, added Mg^{2+}, and very low sucrose concentrations. With no added $MgCl_2$ and at sucrose concentrations of 1% and less, light scattering, sedimentation, and electron microscopy (29, 30) show that a bipolar, octameric minifilament is the stable structure at KCl concentrations between 25 and 75 mM (in addition to about 10 mM imidazole). At higher KCl concentrations, filaments depolymerize, with essentially only monomers observed at about 200 mM and higher. At KCl concentrations lower than optimal, intermediates in minifilament assembly are observed. With no added KCl, an equilibrium between tetrameric and octameric bipolar filaments has been proposed (30). Added Mg^{2+} promotes both the assembly of minifilaments and the lateral aggregation of these thin filaments into thick filaments (29).

The insensitivity of the slow component relaxation time to

myosin concentration, field strength, applied pulse length, and Mg^{2+} concentration, the constant $\Delta a_{rise}/\Delta a_{decay}$ ratio independent of myosin and Mg^{2+} concentrations, and the linear dependence of signal amplitudes on myosin concentration all indicate that intermediate species in the thin filament assembly contribute negligibly to the birefringence under the experimental conditions reported here. Intermediate species are clearly apparent at Mg^{2+} concentrations less than about 0.5 mM in 5% sucrose and up to 2 mM Mg^{2+} in 20% sucrose from changes in the slow relaxation time, from changes in the $\Delta a_{fast}/\Delta a_{slow}$ ratio of amplitudes, and from a nonlinear dependence of signal amplitude on field strength.[2]

Thick filament structure is not well defined. Electron microscopy shows structures with variable widths and lengths that still appear to be bipolar. There is no indication, however, in the birefringence decay kinetics of a second, more slowly relaxing component that would be expected for thick filament formation. Thick filament formation is accompanied by very large increases in light scattering intensity and sedimentation coefficient. At 30 °C, ~0 M KCl, 10 mM imidazole, pH 7.0, and 5% sucrose, Kuznicki *et al.* (14) reported a comparatively small increase in sedimentation coefficient between 1 and 5 mM $MgCl_2$ for both phosphorylated and dephosphorylated myosin filaments. The observed sedimentation coefficient is consistent with estimates for the octameric minifilament structure (29). Between 5 and 7 mM $MgCl_2$, an approximately 4–5-fold increase in sedimentation coefficient was observed for dephosphorylated myosin, indicating thick filament formation. Thick filaments of phosphorylated myosin formed above 7 mM $MgCl_2$. Sinard and Pollard (29) observed an approximately 30-fold increase in light scattering intensity of dephosphorylated and phosphorylated myosin between 0 and 5 mM $MgCl_2$ with no KCl, 8.5 mM imidazole, pH 7.0, and 0.7% sucrose, indicative of a transformation from thin to thick filaments, but noted that higher concentrations of sucrose, as were used here and by Kuznicki *et al.* (14), favored thin filaments. A precise mapping of the thin ↔ thick filament equilibrium by light scattering or sedimentation as dependent on myosin, $MgCl_2$, and sucrose concentrations as well as temperature has not been reported. Although, in general, dephosphorylated myosin forms larger thick filaments (greater light scattering and larger sedimentation coefficients) more readily, *i.e.* at lower Mg^{2+} concentrations, than phosphorylated myosin (14, 29), under the conditions used in the present experiments, *i.e.* 5% sucrose, pH 7.0, and 1–4 mM $MgCl_2$, only thin filaments are expected for both forms of myosin (14). The birefringence signals we observe are then due only to minifilaments with little or no contribution from intermediate species or thick filaments.

For a well defined structure, the longest relaxation observed corresponds to rotational diffusion. Measured decay times can be compared with calculated rotational diffusional coefficients for model structures. Sinard *et al.* (30) have proposed a specific octamer model for the *Acanthamoeba* myosin II minifilament based on electron microscopy. Their structure incorporates a 15-nm stagger between myosin heads and has an overall length of about 230 nm with a central bare zone of about 115 nm between heads with opposite orientation in the bipolar filament. In modeling this for rotational diffusion coefficient calculations, however, there are still several important conformational parameters not accurately known. Calculated rotational relaxation times will depend, for example, on the angular orientation of the globular heads relative to each other and to the long minifilament axis and on the rotational distribution of monomers about the long axis. Additionally, the amino acid sequence of *Acanthamoeba* myosin II predicts a weakened α-helical structure within the rodlike tail region between residues 381 and 406 of the tail, or about 36 nm from the C-terminal end that could act like a hinge (5). This region would then be analogous to the junction between HMM and LMM in skeletal muscle myosin. The angle between these HMM-like regions and the filament axis will significantly affect rotational diffusion coefficients. If we assume a 90° angle between globular heads of a monomer, that heads are coplanar with the coiled α-helical tails, and that monomers alternate by 180° around the fiber axis, then relaxation times for rotation of the long axis can be calculated for different lengths of the octamer and for different angles between the HMM-like regions and the filament axis.

Fig. 12 shows calculated rotational relaxation times as a function of octamer length for 10° and 20° angles between the HMM-like regions and the filament axis. The observed average 220-μs relaxation time corresponds to a 210–220-nm octamer length. This is some 5–10% shorter than estimated by Sinard *et al.* (30), but still within reasonable agreement. A central bare zone of about 95–105 nm would be more consistent with the observed decay time than the 115-nm estimate of Sinard *et al.* (30). If the angle between globular heads is taken as 180°, rather than 90°, then calculated relaxation times are about 15% smaller at each length than shown in Fig. 12, corresponding to an apparent octamer length of about 225–235 nm. Thus, the structure observed by the slow component decay is consistent with the dimensions of the octamer minifilament measured by other means.

We do not know precisely what sort of motions within the minifilament contribute to the fast component kinetics. The coupling of the rise rates, in particular, indicates that the fast component creates a net dipole moment for the rotational orientation of the minifilament. From the amino acid sequence (5), there is a strong permanent dipole extending over the HMM-like region of the myosin II monomer that will interact with an applied electric field. The cancellation of the

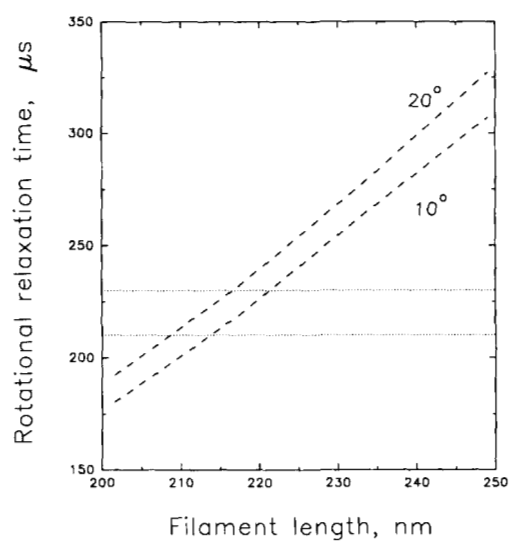

FIG. 12. **The apparent filament length determined from rotational relaxation times.** The dependence of the relaxation time on filament length for two bend angles (10° and 20°) of the HMM-like regions with respect to the long filament axis is shown. Rotational relaxation times are calculated as described by Garcia de la Torre (26) for the octameric minifilament model of Sinard *et al.* (30). Each monomer in the filament is modeled as a set of beads as described in Wijmenga *et al.* (18), with a 90° angle between heads. Filaments are constructed from close packing of monomers that alternate by 180° around the filament. The *dotted lines* show the range of slow component relaxation times observed, 210–230 μs.

[2] M. Riehm and D. C. Rau, unpublished observations.

monomer dipole contributions in a centrosymmetric, bipolar filament structure can be broken by several kinds of internal motions. There are at least two potential sites of flexibility for motion of the HMM-like region, the junction between the globular heads and the rod-like tail and the junction between the HMM-like and LMM-like regions. Bending at the head-tail junction will probably result in a net dipole. Bending or flexing of the whole HMM-like region at the presumed hinge will certainly give a net dipole. There is no clear indication of the range or type of motions possible at these junctions, as, for example, torsional flexing or angular bending that is unidirectional or free within a solid cone. These internal flexing motions can in addition be coupled with two other larger scale motions, a spinning rotation about the filament long axis or an angular redistribution of monomers within the filament. The experimental observation that the fast kinetics show a broad spectrum of relaxation times (Figs. 4 and 9) suggests there are several different motions involved.

Given this complexity of possible internal motions, there is no point in quantitatively fitting the observed birefringence curves to detailed theories. Qualitative results derived for simple models, however, can be compared with our experiments to gain insight into the important features of filament motions. We consider a minimal model that incorporates a range of motions. The filament is modeled as a centrosymmetric, bipolar tetramer (the simplest centrosymmetric, bipolar structure), with HMM-like regions fixed at 180° intervals around the filament, making an angle ϕ_0 with the long axis. Bending or flexing, coplanar with the long filament axis, is assumed to occur at the presumed hinge junction 36 nm from the C terminus. This motion is then coupled to a spinning rotation about the long axis and to the rotation of the long axis. A brief description of the model and final equations for the expected birefringence curves are given in the Appendix (31). Fig. 13 shows a comparison of our experimental data and a theoretical fit. Since we do not have detailed information about monomer dipole moment magnitudes and intrinsic optical factors, amplitudes are simply normalized. The model makes several low level predictions. For small perturbations of the angle between the HMM-like regions and the filament axis, the net dipole induced by flexing will be perpendicular to the long axis (the birefringence of the filament will be negative) for average angles, ϕ_0, less than 35.3°. For stiff springs (the bending force constant for HMM-like region flexing is large compared with thermal energy), the ratio of fast, positive and slow, negative component amplitudes is only dependent on the average angle ϕ_0. The experimentally observed ratio can be fit by the model with a 20–25° angle. Absolute signal amplitudes are inversely proportional to the bending force constant. In the limit of infinitely stiff, symmetrically arranged HMM-like regions, there is, of course, no birefringence signal.

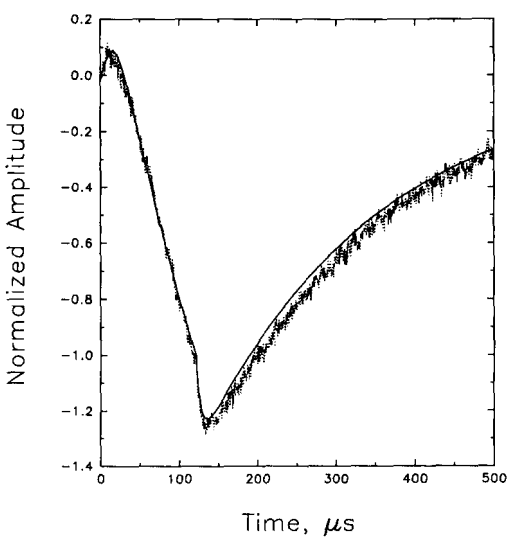

FIG. 13. **Comparison of the observed birefringence signal of filamentous myosin with a minimal theoretical model.** The *dotted curve* shows the birefringence signal observed for phosphorylated myosin filaments at 20 °C in 1 mM KCl, 1 mM imidazole, pH 7.0, 0.5 mM dithiothreitol, 2 mM $MgCl_2$, and 5% sucrose with a 120-μs pulse length. The solid line is calculated from Equations 7–9 in the Appendix (31), with $\phi_0 = 23°$, $\tau_s = 220$ μs, $\tau_f = 20$ μs, and $\tau_\phi = 10$ μs (all relaxation times are for water viscosities at 20 °C). Signal amplitudes of both curves are normalized to −1.0 at the end of the pulse.

The kinetic parameters used in the theoretical fit shown in Fig. 13 are well constrained by experiment. The slowest relaxation time from rotation of the long axis, τ_s of the appendix, is separately fixed by experiment. The spinning relaxation time, that corresponds to the observed fast decay and τ_f of the appendix, is fairly well determined by the time interval between the end of the pulse and the minimum in the birefringence decay and is 20 μs in the fit. Predicted relaxation times for this rotation are very sensitive to the average angle between the HMM-like regions and the long filament axis and to the conformation and disposition of the globular heads. Calculated rotational diffusion coefficients of the structures used for the slow relaxation component indicate that relaxation times for this spinning motion between 5 and 100 μs would be reasonable. The flexing motion kinetics of the HMM-like regions determine the ratio of the rise maximum to decay minimum amplitudes, $\Delta a_{rise}/\Delta a_{decay}$. The fit in Fig. 13 incorporates a bending relaxation time, τ_ϕ of the appendix, of 10 μs. Since the bending force constant is a fundamental factor in this relaxation time, we cannot estimate values from hydrodynamics only. As the bending force constant increases (the spring becomes stiffer), however, the flexing kinetics will become faster and the ratio of the rise maximum to decay minimum will increase. Large changes in the force constant, however, result in comparatively modest changes in the ratio of maximum to minimum amplitudes.

Although this model is not intended as a quantitatively exact treatment, the qualitative features of the experimental data can be well described. This set of coupled motions does provide a framework for understanding the changes in amplitudes and kinetics observed with myosin phosphorylation and Mg^{2+} concentration. The relatively small changes in amplitude and kinetics of the signal from phosphorylated myosin filaments as a function of Mg^{2+} concentration mean that neither the structure nor the flexibility of the filament is changing significantly. The large decrease in amplitude of dephosphorylated myosin minifilaments with added Mg^{2+} can be interpreted as a substantial stiffening of the assembly, *i.e.* the spring constant for flexing of the HMM-like region increases. The 50-fold difference in Δa_{slow} at 4 mM Mg^{2+} (Fig. 9) between phosphorylated and dephosphorylated filaments would correspond to a 50-fold difference in spring constant. In the stiff spring limit, a change in bending force constant would not affect the ratio of fast and slow component amplitudes, $\Delta a_{fast}/\Delta a_{slow}$, as is observed. The absence of any change in the slow relaxation time (rotation of the long axis) and in $\Delta a_{fast}/\Delta a_{slow}$ means that the basic filament structure is unchanged. A significant decrease in flexibility would also explain the observed increase in the ratio of rise maximum to decay minimum amplitudes, from about 0.2 to 0.4. Within the framework of the model, at least an order of magnitude

increase in the bending force constant would be necessary for this change, consistent with the change in slow component amplitudes. In fact, a ratio, $\Delta a_{rise}/\Delta a_{decay}$, of 0.4–0.5 is the maximum expected for infinitely fast, infinitely stiff flexing motions from this model. One shortcoming of the model is that an increase in the fast relaxation time with increased stiffness is not predicted. This simplified model, however, can qualitatively explain many features of the observed birefringence curves.

The actin-activated Mg^{2+}-ATPase activity of assembled *Acanthamoeba* myosin II is sensitively dependent on C-terminal serine phosphorylation (14, 16, 17). Filaments composed of both phosphorylated and dephosphorylated monomers do not show enzymatic activities that are simple linear averages of the two extremes. Phosphorylated monomers have a much greater effect on ATPase activity than expected from their fraction in the filaments. Qualitatively, much the same sort of behavior is observed for the apparent internal flexibility (birefringence amplitudes and fast component kinetics) of copolymeric minifilaments. The almost constant ratio of fast and slow component amplitudes, $\Delta a_{fast}/\Delta a_{slow}$, and the insensitivity of the relaxation time of the slow component to the fraction of phosphorylated monomer indicate that the overall filament structure is unchanged. Those experimental parameters we find connected with internal flexibility, Δa_{slow}, $\langle \tau_{fast} \rangle$, and $\Delta a_{rise}/\Delta a_{decay}$, however, all show a similar nonlinear dependence on fraction phosphorylated monomer. Phosphorylation has a much larger effect on the apparent flexibility than would be anticipated from a linear dependence. The observed variation of slow component amplitudes is better described by a quadratic dependence.

Our previous electric birefringence results (18) for monomers and parallel dimers suggested that an overlap of the phosphorylatable C-terminal region of one monomer with the junction region between the HMM-like and LMM-like domains of a second myosin monomer is perhaps an important feature of filament structure. As already mentioned, this junction is a region of predicted weakened α-helical structure (5). Myosin monomers appear bent at this region in electron micrographs (7), an observation consistent with electric birefringence results (18). The average bend angle was estimated as 110° from the rotational relaxation time of monomers. The results here indicating a substantial difference in internal flexibility between phosphorylated and dephosphorylated filaments could be explained, then, if the junction flexibility of one myosin monomer is regulated by the overlapping C-terminal region of another. Overlap of a junction with a dephosphorylated, C-terminal region would stiffen the junction with increased Mg^{2+}, while a phosphorylated region would have little effect on junction flexibility (up to 4 mM $MgCl_2$). The model presented by Atkinson and Korn (20) based on an overlap between the junction and C-terminal regions further suggests a mechanism for a nonlinear dependence of flexibility on the fraction of phosphorylated myosin in copolymeric filaments. If the model is recast as an octamer, rather than the hexadecamer given by Atkinson and Korn (20), then out of the eight junction regions, four could be involved in a potentially tight coupling of two junctions with two C-terminal regions. If the stiffening of both junctions requires that both C-terminal regions are dephosphorylated, then a quadratic dependence of flexibility on fraction dephosphorylated myosin is expected.

There are striking similarities between the electric birefringence data and the actin-activated Mg^{2+}-ATPase activities for dephosphorylated and phosphorylated myosin II. As mentioned, the greater than linear response of the ATPase activity to the fraction of phosphorylated monomer in copolymers of dephosphorylated and phosphorylated molecules is paralleled by the disproportional response of all of the electric birefringence parameters that are associated with internal flexibility. In addition, it may be more than coincidental that the optimal Mg^{2+} concentration for actin-activated ATPase activity of dephosphorylated myosin II, 4 mM (14), is the concentration at which the amplitude of the major, slow birefringent component approaches zero, or maximal rigidity.

It is reasonable, therefore, to infer a direct causal relationship between the difference in flexibility of the HMM-like arms of dephosphorylated and phosphorylated myosin II filaments and their different actin-activated Mg^{2+}-ATPase activities. Possibly, the flexible HMM-like arms of the phosphorylated filaments are unable to undergo the mechanical events that are normally associated with the hydrolysis of ATP by actomyosin. This would inhibit ATP hydrolysis if the catalytic and mechanical cycles were tightly and necessarily coupled. Consistent with this model is the fact that both phosphorylated and dephosphorylated monomers of *Acanthamoeba* myosin II have full actin-activated Mg^{2+}-ATPase activity (32). The effects of phosphorylation are, however, more complex because neither phosphorylated monomers nor phosphorylated filaments are active in an *in vitro* motility assay (32) and both are more rapidly proteolyzed than their dephosphorylated counterparts by endoproteinase Arg-C at Arg-638 in the globular head (33). Whatever the mechanism, however, the influence of the conformation of the myosin rod on actin-activated Mg^{2+}-ATPase is unlikely to be unique to *Acanthamoeba* myosin II.

REFERENCES

1. Maruta, H., and Korn, E. D. (1977) *J. Biol. Chem.* **252,** 6501–6509
2. Pollard, T. D., Stafford, W. F., III, and Porter, M. E. (1978) *J. Biol. Chem.* **253,** 4798–4808
3. Atkinson, M. A. L., Robinson, E. A., Appella, E., and Korn, E. D. (1986) *J. Biol. Chem.* **261,** 1844–1848
4. Atkinson, M. A. L., and Korn, E. D. (1986) *J. Biol. Chem.* **261,** 3382–3388
5. Hammer, J. A., III, Bowers, B., Paterson, B. M., and Korn, E. D. (1987) *J. Cell Biol.* **105,** 913–925
6. Côté, G. P., Robinson, E. A., Appella, E., and Korn, E. D. (1984) *J. Biol. Chem.* **259,** 12781–12787
7. Kuznicki, J., Côté, G. P., Bowers, B., and Korn, E. D. (1985) *J. Biol. Chem.* **260,** 1967–1972
8. Collins, J. H., and Korn, E. D. (1980) *J. Biol. Chem.* **255,** 8011–8014
9. Collins, J. H., and Korn, E. D. (1981) *J. Biol. Chem.* **256,** 2586–2595
10. Côté, G. P., Collins, J. H. and Korn, E. D. (1981) *J. Biol. Chem.* **256,** 12811–12816
11. Collins, J. H., Côté, G. P., and Korn, E. D. (1982) *J. Biol. Chem.* **257,** 4529–4534
12. Collins, J. H., Kuznicki, J., Bowers, B., and Korn, E. D. (1982) *Biochemistry* **21,** 6910–6915
13. Sathyamoorthy, V., Atkinson, M. A. L., Bowers, B., and Korn, E. D. (1990) *Biochemistry* **29,** 3793–3797
14. Kuznicki, J., Albanesi, J. P., Côté, G. P., and Korn, E. D. (1983) *J. Biol. Chem.* **258,** 6011–6014
15. Baines, I. C., and Korn, E. D. (1990) *J. Cell Biol.* **111,** 1895–1904
16. Atkinson, M. A. L., Lambooy, P. K., and Korn, E. D. (1989) *J. Biol. Chem.* **264,** 4127–4132
17. Ganguly, C., Atkinson, M. A. L., Attri, A. K., Sathyamoorthy, V., Bowers, B., and Korn, E. D. (1990) *J. Biol. Chem.* **266,** 9993–9998
18. Wijmenga, S. S., Atkinson, M. A. L., Rau, D., and Korn, E. D. (1987) *J. Biol. Chem.* **262,** 15803–15808
19. Pollard, T. D. (1982) *J. Cell Biol.* **95,** 816–825
20. Atkinson, M. A. L., and Korn, E. D. (1987) *J. Biol. Chem.* **262,** 15809–15811
21. Pollard, T. D., and Korn, E. D. (1973) *J. Biol. Chem.* **248,** 4682–4690
22. Pardee, J. D., and Spudich, J. A. (1982) *Methods Enzymol.* **85,** 164–181
23. Charney, E. (1988) *Q. Rev. Biophys.* **21,** 1–60
24. Provencher, S. W. (1982) *Comput. Phys. Commun.* **27,** 213–227
25. Provencher, S. W. (1982) *Comput. Phys. Commun.* **27,** 229–242
26. Garcia de la Torre, J., and Bloomfield, V. A. (1981) *Q. Rev. Biophys.* **14,** 81–139
27. Benoit, H. (1951) *Ann. Phys. (Paris)* **6,** 561–609
28. Szabo, A., Haleem, M., and Eden, D. (1986) *J. Chem. Phys.* **85,** 7472–7479
29. Sinard, J. H., and Pollard, T. D. (1989) *J. Cell Biol.* **109,** 1529–1535
30. Sinard, J. H., Stafford, W. F., and Pollard, T. D. (1989) *J. Cell Biol.* **109,** 1537–1547
31. Rau, D. C. (1993) *J. Biol. Chem.* **268,** 4622–4624
32. Ganguly, C., Baines, I. C., Korn, E. D., and Sellers, J. (1992) *J. Biol. Chem.* **267,** 20900–20904
33. Ganguly, C., Martin, B., Bubb, M., and Korn, E. D. (1992) *J. Biol. Chem.* **267,** 20905–20908